Large Variations in the Composition of Ionic Liquid-Solvent Mixtures in Nanoscale Confinement

Alta Fang* and Alex Smolyanitsky*

Applied Chemicals and Materials Division, National Institute of Standards and Technology, Boulder, CO 80305 USA

E-mail: alta.fang@nist.gov; alex.smolyanitsky@nist.gov

Abstract

Mixtures of an ionic liquid with an organic solvent are widely used as electrolytes in supercapacitors, where they are often confined in porous electrodes with pore widths only slightly larger than the sizes of bare ions or solvent molecules. The composition of the electrolyte inside these pores, which may depend on the pore width and choice of electrolyte, can affect supercapacitor performance but remains poorly understood. Here we perform all-atom molecular dynamics simulations of solutions of two different ionic liquids in acetonitrile under confinement between graphene sheets forming slit pores of various widths. We observe significant oscillations in the in-pore ionic liquid mole fraction with varying pore width. Ions are excluded from very narrow pores, while for pore widths that tightly fit a single layer of ions we observe an in-pore ionic liquid mole fraction over three times greater than that in the bulk. At slightly larger pore widths, we observe for different ionic liquids either a nearly complete exclusion of ions from the pore or a slight depletion of ions, while ion population again increases as pore width further increases. We develop an analytical model that can qualitatively predict

1

in-pore ionic liquid mole fraction based on the effective molar volumes and the pore wall interaction energies of each species. Our work suggests a new avenue for tuning the ionic liquid mole fraction in nanopores with potentially significant implications for designing systems involving nanoconfined liquid electrolytes such as supercapacitors, where in-pore ion population can affect charging dynamics.

Keywords

molecular dynamics, nanoscale confinement, slit pores, organic electrolytes, liquid mixtures

Introduction

Mixtures of an ionic liquid with an organic solvent yield a good balance of energy and power performance when used as electrolytes in supercapacitors, due to their moderately high ionic conductivities as well as operating voltages.[1,2] These electrolytes are typically confined in the pores of carbon electrodes, where the confinement region is often smaller than 1 nm, so that resulting pore sizes are only one or two times the diameters of bare ions or solvent molecules.[3,4] Given such confinement, the in-pore composition of ions and solvent may be expected to differ from the bulk,[5] but the molecular details of the partitioning of electrolyte mixtures in very narrow nanopores are not well understood.

The composition of the electrolyte inside a nanoporous electrode can have a significant impact on supercapacitor performance. In-pore ion population has been experimentally shown to correlate with in-pore ion diffusion coefficients, which in turn can affect supercapacitor charging rates.[4] Ionophobic pores (pores that contain very few ions at zero charge) are predicted to lead to enhanced power and energy density in supercapacitors with nanoporous electrodes,[6] although such pores have yet to be observed experimentally.[1] Furthermore, experiments have shown an "anomalous" increase in capacitance when average pore size is reduced below 1 nm.[7,8] Although this large increase in capacitance has been generally at-

tributed to desolation of ions in very narrow pores,[3,9,10] there have been few theoretical studies of confined electrolyte mixtures containing a neutral solvent.[9–11] Existing models have simulated electrolytes in disordered electrodes using coarse-grained molecular dynamics (MD),[9] used continuum theories,[10] or focused on aqueous electrolytes.[11]

Although theoretical work on highly confined liquid mixtures has been limited in the context of supercapacitors, several publications in the 1990s reported oscillatory behavior of the equilibrium composition of mixtures of different-sized spherical molecules as a function of pore width, motivated by applications such as the use of zeolites for separations.[12–14] Indeed, "superselectivity," which is when a pore is highly selective for the smaller of the two spherical molecules that can fit into it, was observed in both Monte Carlo simulations[13] and a statistical mechanical treatment of hard rod mixtures.[15] A layer packing factor was introduced to help explain the preferred molecular packing arrangements inside a pore.[12] However, these models have thus far been limited to simple systems such as spherical Lennard-Jones or hard sphere molecules,[14] and the literature in this area has not been well-connected with the recently growing field of nanoconfined electrolytes for energy storage applications.

Here we perform all-atom molecular dynamics simulations of 1.5 M solutions of two ionic liquids in acetonitrile (ACN) confined between graphene sheets forming slit pores of different widths. Each carbon atom in the graphene sheets carries fixed zero charge. Figure 1(a) shows a schematic of the simulated system, which is comprised of a bulk liquid reservoir in contact with a narrow slit pore defined by two parallel graphene sheets, with perpendicular graphene sheets as reservoir walls. The slit pore geometry used here has also been used previously in other molecular simulation studies of nanoconfined electrolytes[6] and represents a simplified model of a pore in a nanoporous carbon electrode. Figure 1(b) shows the structures of the species studied. The two ionic liquids in the present study differ in the anion; 1-ethyl-3-methylimidazolium (EMIM$^+$) is combined with either bis(trifluoromethylsulfonyl)imide (TFSI$^-$) or tetrafluoroborate (BF$_4^-$). These liquids are chosen since they are commonly studied supercapacitor electrolytes,[2,17] and a concentration of 1.5 M is chosen for consis-
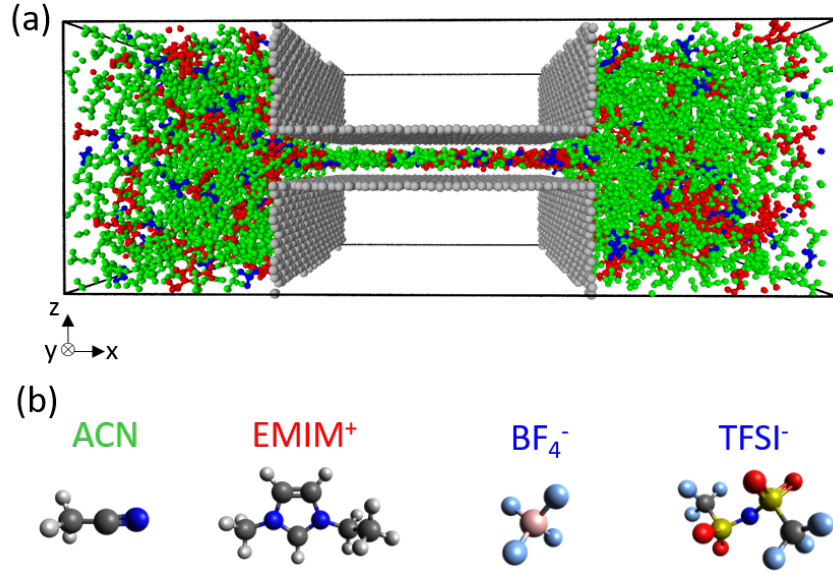
Figure 1: (a) Schematic of our simulation setup, shown here for 1.5 M [EMIM$^+$][BF$_4^-$] in acetonitrile and a pore of width of 0.84 nm. Acetonitrile, EMIM$^+$, BF$_4^-$, and wall carbons are shown in green, red, blue, and gray respectively. Image was rendered using OVITO.[16] (b) Structures of the species comprising the studied liquids.

tency with published studies of ionic liquid-acetonitrile mixtures used as supercapacitor electrolytes.[3,4]

We study slit pore widths ranging from 0.76 nm to 1.32 nm, where the pore width w is defined as the center-to-center distance between the graphene sheets comprising the pore walls. This range of values is chosen to focus on the regime where the pore contains one or two layers of liquid molecules. For each simulation, we characterize the equilibrium in-pore ionic liquid mole fraction $X_{IL} = \dfrac{N_{IL}}{N_0 + N_{IL}}$, where $N_{IL} = \frac{1}{2}(N_+ + N_-)$ is the average number of ions and N_0 is the average number of solvent molecules in the pore, calculated using the center of mass of each molecule. To reduce edge effects, we define the inside of the pore to be the region to the interior of 1 nm from the pore mouth on each side [see Fig. S1 in the Supporting Information (SI) for more information].
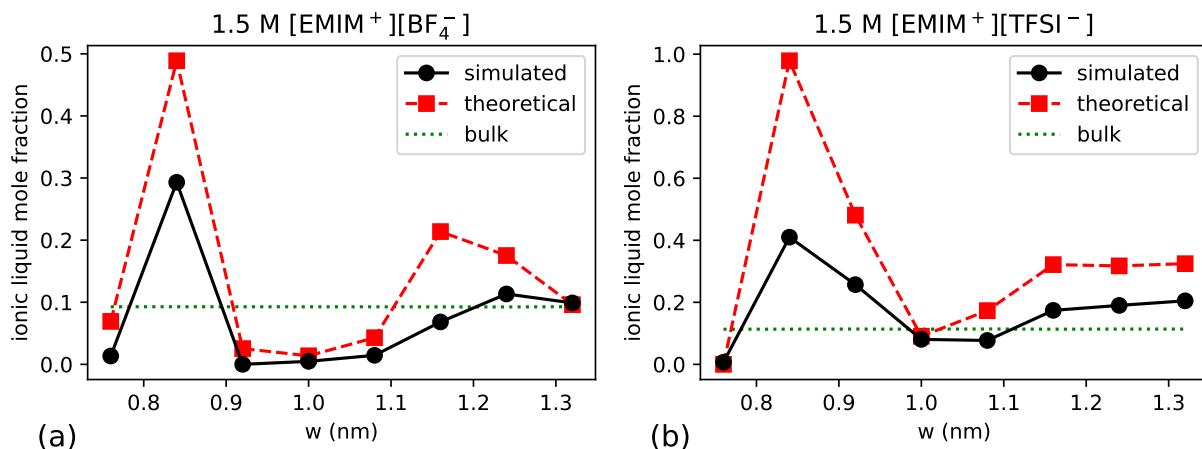
Figure 2: In-pore ionic liquid mole fraction as a function of pore width, from MD simulations (black circles) and theoretical predictions (red squares) for (a) 1.5 M [EMIM$^+$][BF$_4^-$] and (b) 1.5 M [EMIM$^+$][TFSI$^-$] in acetonitrile. The bulk ionic liquid mole fractions are shown as green dotted lines for comparison. The standard deviations of the simulated data from block averaging[18] over 2-ns blocks are smaller than the symbol size, and uncertainties associated with how the in-pore region is defined can be inferred from Fig. S1 in the SI.

Results and Discussion

Figures 2(a) and (b) show simulated in-pore X_{IL} for 1.5 M [EMIM$^+$][BF$_4^-$] and 1.5 M [EMIM$^+$][TFSI$^-$] in acetonitrile respectively (black circles). For both mixtures, the simulated in-pore ionic liquid mole fraction exhibits a clear peak at $w = 0.84$ nm, which is followed by a relative minimum near $w = 1$ nm and then an increase in X_{IL} for larger pore widths. Figures S2 and S3 in the SI show top-down views of simulation snapshots of each mixture confined in each pore.

For the narrowest pore width considered, our simulations show that for both liquids there are almost no ions in the pore and the pore is almost entirely filled with solvent. For 1.5 M [EMIM$^+$][TFSI$^-$], this occurs because TFSI$^-$ is too large to fit in the pore, as confirmed by a separate simulation in which pure [EMIM$^+$][TFSI$^-$] was unable to enter a pore of width 0.76 nm. On the other hand, a separate simulation showed that pure [EMIM$^+$][BF$_4^-$] was able to enter a pore of width 0.76 nm, so the depletion of ions in the mixture at this pore width is driven not strictly by steric hindrance but rather by the relative energetic favorability of
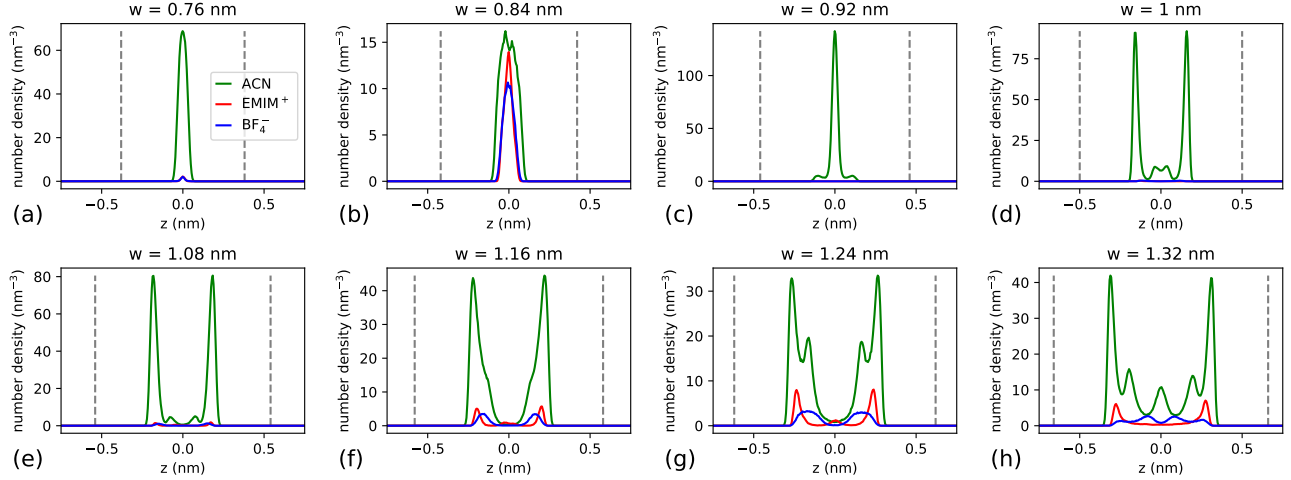
5

Figure 3: Center-of-mass number density profiles of each species across the width of the pore for 1.5 M [EMIM$^+$][BF$_4^-$] in acetonitrile confined in pores of various widths. Dashed vertical lines indicate the positions of the center planes of the pore walls.

filling the pore with acetonitrile.

For a pore width of 0.84 nm, in both mixtures we observe an over threefold greater ionic liquid mole fraction in the pore compared to in the bulk. This occurs because a single layer of ions is able to fit relatively well in a pore of this width, so that a greater fraction of ions leads to a more favorable average in-pore energy density. At $w = 0.92$ nm, the two mixtures behave quite differently, as will be discussed further below. When $w = 1$ nm or 1.08 nm, the ability of acetonitrile molecules to pack efficiently in two layers while the ions can only form one loosely fitting layer contributes to the observed reduction in in-pore ionic liquid mole fraction for both mixtures. Less depletion of ions is observed for the mixture containing TFSI$^-$ than for the mixture with BF$_4^-$ since the larger TFSI$^-$ has a stronger attractive interaction with the pore walls and may also be able to achieve a better fit in these pores. Finally, as the pore width increases to 1.16 nm and higher, X_{IL} increases again for both liquids, driven by the relatively favorable energy density achieved in the pore by two layers of ions compared to two layers of solvent, although the enrichment in ions at these larger widths is much less pronounced than at $w = 0.84$ nm.

The center-of-mass number density profiles of each species across the width of the pore are
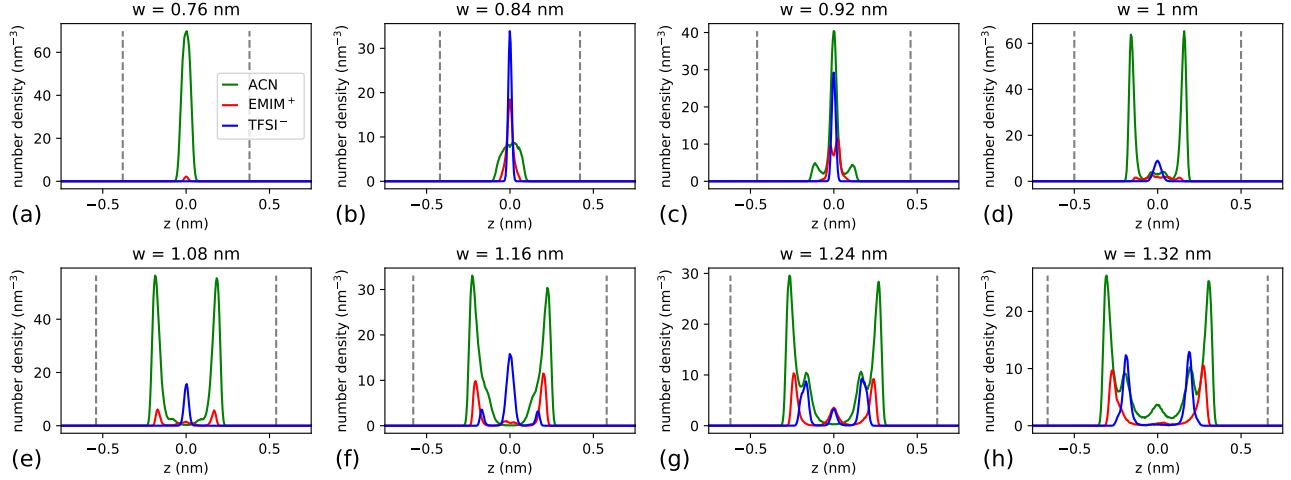
Figure 4: Center-of-mass number density profiles of each species across the width of the pore for 1.5 M [EMIM$^+$][TFSI$^-$] in acetonitrile confined in pores of various widths. Dashed vertical lines indicate the positions of the center planes of the pore walls.

shown in Figs. 3 and 4 for 1.5 M [EMIM$^+$][BF$_4^-$] and 1.5 M [EMIM$^+$][TFSI$^-$] respectively, clearly demonstrating the layered structure of the liquid in the pores. In both mixtures, acetonitrile forms a single layer (reflected by a single peak in the number density) in pores up to 0.92 nm in width and at least two layers in pores from 1 nm to 1.32 nm in width. The ions, if present, form a single layer in pores narrower than $\sim$1 nm and at least two layers in the wider pores.

To help interpret the simulated data, we develop an analytical theory describing the in-pore ionic liquid mole fraction as a function of pore width. Previously, classical density functional theory approaches have been used to model the behavior of concentrated electrolyte mixtures in confinement.[10,19,20] Here, for qualitative illustration we instead present an approach based on Flory-Huggins solution theory[21] and focus on modeling the volume-averaged concentration of each species within the pore rather than attempt to describe the spatial distribution of the molecular densities across the pore.

Let c_i represent the average in-pore concentration of species i. We assume that electroneutrality is obeyed overall in the pore, since the estimated Debye length of the considered electrolytes is smaller than the effective molecular dimensions and we also observe in each

7

MD simulation that the magnitude of the total charge of the confined liquid per pore area is less than 0.03 e/nm^2 (where e is the elementary charge). Thus, the average concentrations of cations and anions, which here are both monovalent, are assumed to be equal inside an uncharged pore, so we define the in-pore ionic liquid concentration as

$$c_{\text{IL}} \equiv c_+ = c_- \tag{1}$$

and the in-pore solvent concentration as c_0.

The excess Gibbs energy density f_{tot} of a liquid inside a pore relative to bulk liquid can be expressed as:

$$f_{tot} = \sum_{i\in\{0,+,-\}} U_i c_i + k_B T \left[\sum_{i\in\{0,+,-\}} c_i \ln(c_i v_i) + \alpha c_0 v_0 c_{\text{IL}} v_{\text{IL}} \right] - \sum_{i\in\{0,+,-\}} \mu_i^\infty c_i. \tag{2}$$

Equation 2 represents the sum of the species-wall interaction energies, the entropy of mixing, and the enthalpy of mixing (treating the liquid as a binary mixture of ionic liquid and solvent for simplicity), relative to the Gibbs energy density of a bulk liquid.[22] Here, U_i is the average per-molecule interaction energy of species i with the pore walls, v_i is the effective molar volume of species i accounting for molecular layering and packing behavior in the pore (where $v_{\text{IL}} \equiv v_+ + v_-$ is the effective molar volume of the ionic liquid), k_B is Boltzmann's constant, T is the temperature, α is a mixing energy density parameter (proportional to the commonly used Flory-Huggins χ parameter),[23] and μ_i^∞ is the chemical potential of species i in the bulk. All variables are functions of the pore width w except for k_B, T, and μ_i^∞, but for brevity we will not explicitly write out functional dependences on w. For a discussion on using total energy and per-area wall interaction energies instead of energy density and per-molecule wall interaction energies, see the SI.

The equilibrium concentrations in the pore c_i are then obtained by minimizing f_{tot} with respect to the in-pore concentration of either species.[22] The concentrations are related be-

8

cause the sum of the volume fractions of each species in the pore is equal to one:

$$c_0 v_0 + c_{\mathrm{IL}} v_{\mathrm{IL}} = 1. \tag{3}$$

Thus, using Eq. 3, we can first substitute $c_0 = \dfrac{1 - c_{\mathrm{IL}} v_{\mathrm{IL}}}{v_0}$ into Eq. 2 and then set

$$
\begin{aligned}
0 &= \frac{df_{tot}}{dc_{\mathrm{IL}}} \\
&= -U_0 \frac{v_{\mathrm{IL}}}{v_0} + U_+ + U_- \\
&\quad + k_B T \left[2 + \ln(c_{\mathrm{IL}} v_+) + \ln(c_{\mathrm{IL}} v_-) - \frac{v_{\mathrm{IL}}}{v_0} \ln(1 - c_{\mathrm{IL}} v_{\mathrm{IL}}) - \frac{v_{\mathrm{IL}}}{v_0} + \alpha v_{\mathrm{IL}}(1 - 2c_{\mathrm{IL}} v_{\mathrm{IL}}) \right] \\
&\quad - \Delta \mu^\infty
\end{aligned}
\tag{4}
$$

where

$$\Delta \mu^\infty = \mu_+^\infty + \mu_-^\infty - \mu_0^\infty \frac{v_{\mathrm{IL}}}{v_0}. \tag{5}$$

For $\Delta \mu^\infty$ we use the bulk limit of Eq. 4:

$$
\begin{aligned}
\Delta \mu^\infty &= k_B T \left[2 + \ln(c_{\mathrm{IL}}^\infty v_+^\infty) + \ln(c_{\mathrm{IL}}^\infty v_-^\infty) - \frac{v_{\mathrm{IL}}^\infty}{v_0^\infty} \ln(1 - c_{\mathrm{IL}}^\infty v_{\mathrm{IL}}^\infty) - \frac{v_{\mathrm{IL}}^\infty}{v_0^\infty} \right. \\
&\quad \left. + \alpha v_{\mathrm{IL}}^\infty (1 - 2c_{\mathrm{IL}}^\infty v_{\mathrm{IL}}^\infty) \right],
\end{aligned}
\tag{6}
$$

where c_i^∞ and v_i^∞ are the bulk concentrations and molar volumes of species i.

Separate bulk MD simulations of the pure liquids and 1.5 M ionic liquid mixtures are used to estimate α via

$$\alpha = \frac{\Delta E_{ex}}{v_{mix} k_B T \phi_0 \phi_{\mathrm{IL}}}, \tag{7}$$

where $\Delta E_{ex} = E_{mix} - E_0 X_0 - E_{\mathrm{IL}} X_{\mathrm{IL}}$ is the molar enthalpy of mixing; X_i, E_i, and ϕ_i are the mole fraction, molar potential energy, and volume fraction of liquid i; and v_{mix} is the molar

volume of the mixture. For simplicity we use this bulk value of α in Eq. 4 for all values of pore width, although in a very narrow pore α would probably be less than that in the bulk due to the lower liquid-liquid coordination numbers induced by confinement. Figures S4 and S5 in the SI show that trends in the in-pore ionic liquid mole fraction remain qualitatively similar for different values of $\Delta\mu^\infty$ and α.

To obtain predictions for the in-pore ionic liquid mole fraction $X_{\mathrm{IL}}(w) \equiv \dfrac{c_{\mathrm{IL}}}{c_0 + c_{\mathrm{IL}}}$, U_i and v_i are calculated from MD simulations as described in greater detail below, and Eq. 4 is solved for c_{IL} numerically using a root-finding algorithm. Once c_{IL} is obtained, c_0 can be found using Eq. 3.

As shown in Fig. 2, the analytical theory (red squares) is able to reproduce the qualitative behavior of the simulated X_{IL} well for both mixtures, although it tends to overpredict the fraction of ions. We note that there may be significant uncertainty in our simulation results with the highest in-pore ionic liquid mole fractions because the in-pore counts of each species become limited due to the larger effective volumes of the ions and the slow in-pore diffusion may mean steady state has not actually been reached at the simulated timescales. Another possible source of discrepancy is that the analytical theory neglects changes in the conformational entropy of the ions and solvent molecules upon confinement, which would be expected to disfavor the presence of larger species (here, the ions) in the pores. Also, for pores wide enough to fit at least one layer of solvent alongside one layer of ions, our estimates for v_i used as input into the theory may not accurately capture the packing arrangements of mixtures since here v_i were calculated from separate simulations of the pure liquids.

Overall, the good qualitative agreement between the analytical model and the simulations suggests that the composition of liquid mixtures in very narrow pores is largely governed by an interplay between the pore wall interaction energies and the effective sizes of each species, which are in turn affected by their orientations and layering behavior in the pore, as described in greater detail below. Although smaller species tend to experience a lower magnitude of pore wall attraction, they can pack more efficiently in pores of certain widths,
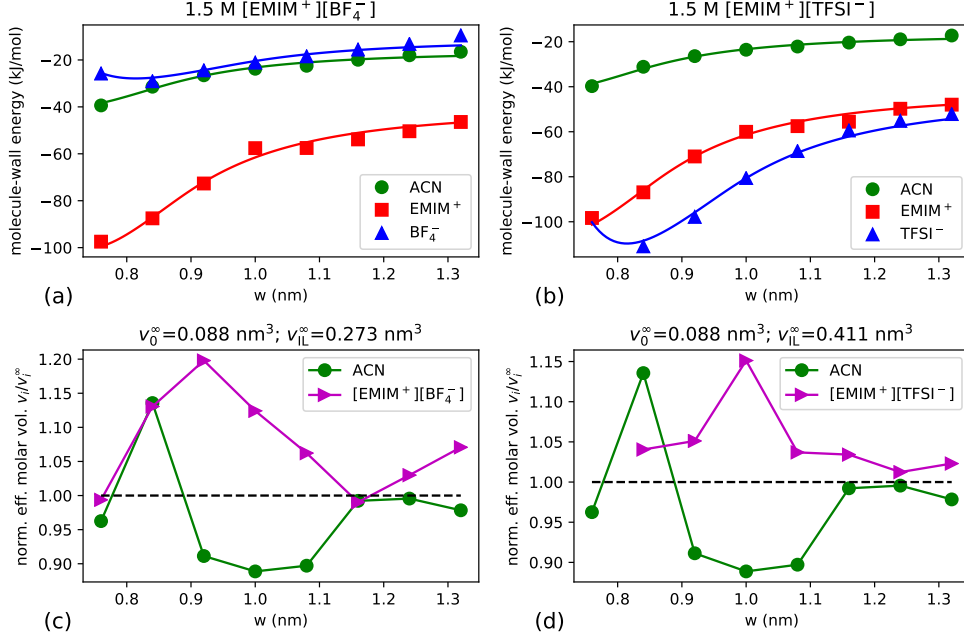
10

Figure 5: (a, b) Average per-species intermolecular interaction energy with the pore walls as a function of pore width. Points are from MD simulations and curves are fits to Eq. S4. (c, d) Effective molar volumes v_i normalized by bulk molar volumes v_i^∞, for various pore widths. (a), (c) are for 1.5 M [EMIM$^+$][BF$_4^-$], while (b), (d) are for 1.5 M [EMIM$^+$][TFSI$^-$]. The bulk molar volumes are shown above subplots (c) and (d).

allowing "superselectivity" to occur under appropriate conditions. Consistent with earlier reports,[5,13] our results demonstrate that not only are differences in the effective sizes of the species in a mixture critical for observing oscillations in in-pore mixture composition, but the pore wall interactions of each species are also important.

Figure 5 shows the simulated values for U_i and v_i (points) used as input in Eq. 4. Figures 5(a) and (b) plot the average per-species intermolecular interaction energy with the pore walls U_i, extracted from simulations of 1.5 M [EMIM$^+$][BF$_4^-$] and 1.5 M [EMIM$^+$][TFSI$^-$] in acetonitrile respectively. The values for the ions at $w = 0.92$ nm in Fig. 5(a) were obtained from a separate simulation of pure [EMIM$^+$][BF$_4^-$] since there were no ions in the pore for the mixture at that pore width. As expected, larger species are generally more strongly attracted to the pore walls, and the magnitude of this attraction generally decreases as the pore becomes wider and each ion or solvent molecule on average resides further from the

11

walls. We have also developed an expression for $U_i(w)$ in this regime of pore widths, as described in the SI, and the curves in Figs. 5(a) and (b) are fits of Eq. S4 to the simulated data. Excellent agreement is obtained, and fitted values for σ_i and ε_i are given in Table S1 in the SI. These values are reflective of the respective sizes and interaction energies of each species with a single flat wall, demonstrating that Eq. S4 may be used to estimate $U_i(w)$ for other species simply by knowing these effective Lennard-Jones parameters. $U_i(w)$ can in turn be used in Eq. 4 to estimate $X_{\mathrm{IL}}(w)$, if $v_i(w)$ is also known.

Figures 5(c) and (d) show v_i/v_i^∞ for each species i, with bulk molar volumes v_i^∞ shown above each plot. Values of v_i are calculated from separate simulations of pure acetonitrile or pure ionic liquid in slit pores via $v_i \equiv \dfrac{L_x L_y (w - \sigma_C)}{N_i}$, where L_x and L_y are the lengths of the pore in the x and y directions respectively, $\sigma_C = 0.355$ nm is used to approximate the diameter of the wall carbon atoms, and the number of molecules N_i is calculating by dividing the number of atoms in the pore by the number of atoms per molecule. No data is shown for [EMIM$^+$][TFSI$^-$] at $w = 0.76$ nm because that ionic liquid is unable to enter such narrow pores. For the ionic liquids, after calculating $v_+ + v_-$ from the MD simulations, separate values for v_+ and v_- are estimated by assuming $v_+/v_- = 4.63$ for [EMIM$^+$][BF$_4^-$] and $v_+/v_- = 0.58$ for [EMIM$^+$][TFSI$^-$], which are based on previous estimates of the ion diameters.[17,24] The choice of v_+/v_- has a negligible effect on theoretically predicted values of X_{IL}.

Due to confinement within the narrow slit pores, the ions and solvent molecules adopt layered configurations and preferred orientations, leading to variations in the effective molar volume as a function of pore width. In Figs. 5(c) and (d), the relatively low values of v_i/v_i^∞ for each species at the narrowest pore width are a result of a single layer of molecules lying flat against the pore walls and fitting tightly in the pore. The effective molar volume increases to a maximum (at $w = 0.84$ nm for ACN, 0.92 nm for [EMIM$^+$][BF$_4^-$], and 1.0 nm for [EMIM$^+$][TFSI$^-$]) as the pore becomes slightly wider than a single layer of flat-lying molecules but not wide enough to accommodate either a single layer of molecules in another

orientation or two layers of molecules, leading to inefficient packing in the pore. As the pore width increases, the effective molar volume then decreases to a minimum as a tight fit is again achieved, either by a single layer of molecules with their longer axis perpendicular to the pore walls in the case of acetonitrile at $w = 0.92$ nm, or two layers of molecules flat against the pore walls in the case of acetonitrile at $w = 1.0$ and 1.08 nm and the ionic liquids around $w = 1.16$ nm or 1.24 nm. Finally, at higher pore widths the effective molar volume increases again as the pore becomes larger than the minimum for two layers but not wide enough to fit three layers.

Although the shape of the $v_i/v_i^\infty(w)$ curves for acetonitrile in Figs. 5(c) and (d) strongly resembles that of $X_{\mathrm{IL}}(w)$ in Fig. 2(a), we note that the effective molar volume of acetonitrile is not the sole predictor of in-pore mixture composition. Figure S6 in the SI shows that using bulk values for v_i instead of effective molar volumes in Eq. 4 still leads to a peak in theoretically predicted in-pore X_{IL} at $w = 0.84$ nm for both mixtures, although otherwise the trends are no longer well predicted. Also, acetonitrile is present in both mixtures studied, but at $w = 0.92$ nm, the value of X_{IL} differs significantly between the two mixtures. This suggests that the lower magnitude of ion-wall attraction of BF_4^- compared to TFSI^- contributes to the observed depletion of ions in the 1.5 M $[\mathrm{EMIM}^+][\mathrm{BF}_4^-]$ mixture at $w = 0.92$ nm, highlighting the importance of the values of each species' pore wall interactions.

In Fig. 6 we plot the in-pore orientations of the acetonitrile molecules, characterized using the average orientational order parameter $\langle P_2(\cos\theta)\rangle = \langle \frac{1}{2}(3\cos^2\theta - 1)\rangle$, where θ is the angle between the normal to the pore walls (the z-axis) and the dipole of the acetonitrile molecule, here calculated as the vector between the sp^3 carbon and the nitrogen. $\langle P_2(\cos\theta)\rangle = 1$ ($\langle P_2(\cos\theta)\rangle = -0.5$) indicates that all of the acetonitrile dipoles are perpendicular (parallel) to the pore walls, while $\langle P_2(\cos\theta)\rangle = 0$ indicates that acetonitrile molecules are oriented randomly, as they are in bulk liquid. For pore widths of 0.76 nm and 0.84 nm, the acetonitrile dipoles are largely aligned parallel to the pore walls, as expected since the pores are too narrow to fit a perpendicular orientation. For a pore width of 0.92 nm, the acetonitrile
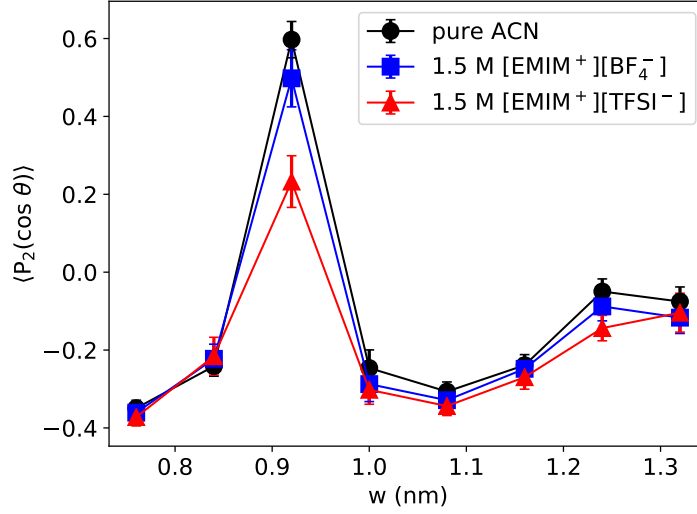
Figure 6: In-pore acetonitrile orientational order parameter $\langle P_2(\cos\theta)\rangle$ as a function of pore width w, for pure acetonitrile, 1.5 M [EMIM$^+$][BF$_4^-$], and 1.5 M [EMIM$^+$][TFSI$^-$]. Points are averages and error bars are standard deviations computed from simulation configurations every 100 ps.

dipoles are primarily oriented perpendicularly to the pore walls, allowing a single layer of acetonitrile molecules to efficiently fill the pore, explaining the relatively low effective molar volume of acetonitrile at $w = 0.92$ nm in Figs. 5(c) and (d). At this width, acetonitrile is relatively less perpendicularly aligned in 1.5 M [EMIM$^+$][TFSI$^-$] than in pure acetonitrile or the mixture containing BF$_4^-$, which is likely due to the higher in-pore ion population for 1.5 M [EMIM$^+$][TFSI$^-$]. Finally, for pore widths of 1 nm to 1.32 nm, the acetonitrile dipoles again orient parallel to the walls, with $\langle P_2(\cos\theta)\rangle$ approaching 0 as w increases and the influence of the walls on the molecular orientations is reduced.

While direct comparisons of our simulation results with experiments are challenging due to the distribution of pore sizes and shapes in disordered nanoporous carbons, nuclear magnetic resonance measurements have shown for 1.87 M solutions of [EMIM$^+$][TFSI$^-$] in acetonitrile that the ionic liquid mole fraction within the pores of the commercial activated carbon YP50F was approximately 30% greater than in the bulk liquid.[25] Given the pore size distribution of YP50F,[4] our simulation results could potentially be used to help interpret these observations, although it has also been found that only ~42% of the pore volume

measured by nitrogen gas sorption was occupied by the electrolyte,[25] so not all pores can be assumed to be accessible to the liquid. Surface force balance measurements[26,27] and X-ray diffraction[28] may provide other opportunities to experimentally probe liquid mixtures under confinement and link simulations with experiments.

Conclusion

In summary, our all-atom MD simulations of ionic liquid-solvent mixtures confined in slit nanopores have shown that the in-pore composition of an electrolyte mixture can vary significantly with pore width when pores contain only one or two liquid layers. These oscillations in in-pore population are driven by an interplay between the packing of the species inside the pore and the pore wall interactions of each species. For both 1.5 M $[EMIM^+][BF_4^-]$ and 1.5 M $[EMIM^+][TFSI^-]$ in acetonitrile, the in-pore ionic liquid mole fraction ranges from nearly zero to over three times its value in the bulk as pore width increases from 0.76 nm to 0.84 nm, before decreasing to a local minimum for pore widths near 1 nm and then increasing again for wider pores. Strikingly, for the 1.5 M $[EMIM^+][BF_4^-]$ solution, ions are nearly completely excluded from pores with widths near 1 nm, while for 1.5 M $[EMIM^+][TFSI^-]$ there is only a slight depletion of ions. We developed an analytical model that qualitatively reproduces the simulated results, demonstrating that the observed trend in in-pore liquid composition can be theoretically predicted based on the effective molar volumes and attractive pore wall interaction energies of each species. Number density profiles of each species across the pore as well as acetonitrile orientations as a function of pore width were also characterized, confirming the significant in-pore structuring of these highly confined liquids.

Although here we have focused on slit pores, in practice, disordered nanoporous carbons used as supercapacitor electrodes can have a variety of pore shapes and significant pore wall curvature.[9] Monte Carlo simulations of mixtures of spherical particles have shown oscillations in the in-pore mixture composition in cylindrical and spherical as well as slit pores,[13]

suggesting qualitatively similar behavior for different degrees of pore curvature, but the effect of pore shape remains to be seen for the non-spherical species considered here. Also, in many nanoporous carbons, liquid commonly wets both sides of the pore walls,[1] unlike in our simulated system. Based on preliminary MD simulations we performed of several layers of liquid-separated graphene sheets alongside a bulk reservoir, we expect that when liquid is on both sides of the pore walls, the observed trends in in-pore mixture composition remain qualitatively similar, although in-pore compositions become closer to that in the bulk. Finally, accounting for the polarizability of conductive pore walls using the more computationally expensive constant-potential method[29,30] rather than the constant-charge method may result in slightly higher in-pore ionic liquid mole fractions,[31] but we expect observed qualitative trends to remain the same, particularly since our systems involve uncharged pores and steady-state conditions.

Our work demonstrates that in very narrow pores, not only is ion desolvation possible, as previously suggested,[3,9,10] but a considerable increase in ion solvation is also possible, so that a wide range of pore ionophobicities or ionophilicities can in principle be achieved for a single electrolyte mixture by simply varying pore width. In practice, non-negligible spread in the pore size distributions of real materials is inevitable, and controlling in-pore mixture composition by engineering pore geometry would undoubtedly be challenging. Nonetheless, our simulations and analytical theory may be useful for informing the design of systems involving nanoconfined liquid mixtures such as supercapacitors or separation membranes. Additionally, although here we have not studied charged pores, our observations of large variations in in-pore electrolyte composition with pore size may also potentially be relevant to the "anomalous" capacitance increase observed in supercapacitors with subnanometer pores,[3,8] since charging rates and mechanisms could be affected by pore width via differences in initial ion populations, for example. Furthermore, our findings indicate that in-pore electrolyte composition is likely to be highly heterogeneous in a real disordered nanoporous electrode with a range of pore sizes. More broadly, given the existence of numerous possible

combinations of miscible solvents and ionic liquids, each featuring different sets of molecular sizes, shapes, and interaction energies, our results suggest potentially significant new opportunities for tuning the composition of liquid mixtures under confinement by tuning pore size and molecular properties.

Methods

We perform all-atom MD simulations using GPU-accelerated LAMMPS (version 16 Mar. 2018),[32–34] and initial configurations for the liquid are generated using Packmol.[35] The ions are modeled using the all-atom OPLS-based force field of Ref. 36 with charges scaled by a factor of 0.8, and acetonitrile is modeled using the force field parameters of Ref. 37 within an OPLS force field form (see SI for acetonitrile parameters used). The Lennard-Jones parameters for the carbon atoms of the pore walls are modeled with OPLS values of $\varepsilon = 0.29288$ kJ/mol and $\sigma = 0.355$ nm,[38] and a lattice constant of $a = 0.246$ nm is used for the graphene sheets. Long-range Coulombic interactions are calculated using a particle-particle particle-mesh (PPPM) solver. A cutoff distance of 1.2 nm is used for the Lennard-Jones and real-space Coulombic interactions, and a 1 fs timestep is used.

All charges on the pore wall atoms are fixed to zero, which neglects polarizability of the pore walls.[29–31] During equilibration in the NPT ensemble, the wall carbon atom positions are fixed in space, while during the NVT simulations they are restrained using springs with a spring constant of 332 N/m. Periodic boundary conditions are used in all directions. The length of the simulation box is 5.96 nm in the y direction and ranges from 3.96 nm to 4.52 nm in the z direction. The length of the slit pore in the x direction is 4.69 nm, and we initialize the system with a total number of ions and solvent molecules such that once the pore is filled the length of the bulk liquid in the x direction is at least 5.5 nm. These dimensions were chosen to balance in-pore ensemble size with the need for significant simulation times. During production simulations, there are on average 47 to 161 total ions

plus solvent molecules inside each pore (after discarding 1 nm from the pore mouth in each direction).

The systems are initialized with bulk liquid adjacent to an unfilled pore. For the ionic liquid-solvent mixtures, we then simulate the system in the NPT ensemble for 2 ns, during which the pore spontaneously fills with liquid. The temperature is maintained at 300 K by a stochastic velocity rescaling thermostat with a time constant of 100 fs, and the pressure is maintained at 101.325 kPa by a Berendsen barostat coupled to the box length in the x direction, while keeping the box dimensions in the y and z directions fixed, with a 1 ps time constant and a compressibility of 0.4545 GPa^{-1}. Next, the system is equilibrated in the NVT ensemble at a temperature of 300 K over a time ranging from 10 ns to 90 ns, depending on the pore width. For some pore widths, a significant amount of equilibration time is required for the in-pore liquid composition to reach steady state, since the mixture composition inside the pore may change significantly after the initial rapid filling of the pore (see Fig. S10 in the SI). Plots of the in-pore number density of each species as a function of time are visually inspected to evaluate whether a system has sufficiently equilibrated. Finally, production simulations are performed for 10 ns in the NVT ensemble. For simulations of pure acetonitrile (pure ionic liquid) in confinement, we use the same procedure with at least 2 ns (4 ns) of NPT equilibration, followed by 2 ns (5 ns) of NVT equilibration, and then 4 ns (5 ns) of NVT production simulation. To obtain bulk molar volumes of each species, we perform bulk simulations of pure acetonitrile or pure ionic liquid in the NPT ensemble with 0.5 ns of equilibration using a stochastic velocity rescaling thermostat and Berendsen barostat, followed by 1.5 ns of equilibration and then 2 ns of production simulation using a Nose-Hoover thermostat and barostat. To estimate α, the molar potential energy is calculated from 2 ns of NVT simulation of bulk pure or mixed liquids following 2 ns of NPT equilibration.

Acknowledgement

Disclaimer

This work is a contribution of the National Institute of Standards and Technology, an agency of the US government. Not subject to copyright in the USA. Trade names are provided only to specify procedures adequately and do not imply endorsement by the National Institute of Standards and Technology. Similar products by other manufacturers may be found to work as well or better.

Supporting Information Available

- supporting_information.pdf: Effects of varying in-pore region definition; top-down views of mixtures inside the slit pores; theoretically predicted $X_{\text{IL}}(w)$ for different values of $\Delta\mu^\infty$, α, or v_i; model for $U_i(w)$, with fitted values for σ_i and ε_i; discussion of using total energy and per-area wall interaction energy in the analytical theory; force field parameters for acetonitrile; examples of time evolution of in-pore species counts.

- SI_movie1.avi: Movie of in-pore liquid for 1.5 M $[\text{EMIM}^+][\text{BF}_4^-]$ in acetonitrile confined in a pore of $w = 1$ nm, showing top-down view over the entire NVT simulation (40 ns).

- SI_movie2.avi: Movie of in-pore liquid for 1.5 M $[\text{EMIM}^+][\text{TFSI}^-]$ in acetonitrile confined in a pore of $w = 0.92$ nm, showing top-down view over the entire NVT simulation

(60 ns).

References

(1) Forse, A. C.; Merlet, C.; Griffin, J. M.; Grey, C. P. New Perspectives on the Charging Mechanisms of Supercapacitors. *J. Am. Chem. Soc.* **2016**, *138*, 5731–5744.

(2) Vatamanu, J.; Borodin, O.; Olguin, M.; Yushin, G.; Bedrov, D. Charge Storage at the Nanoscale: Understanding the Trends from the Molecular Scale Perspective. *J. Mat. Chem. A* **2017**, *5*, 21049–21076.

(3) Chmiola, J.; Largeot, C.; Taberna, P.-L.; Simon, P.; Gogotsi, Y. Desolvation of Ions in Subnanometer Pores and Its Effect on Capacitance and Double-Layer Theory. *Angew. Chem., Int. Ed.* **2008**, *47*, 3392–3395.

(4) Forse, A. C.; Griffin, J. M.; Merlet, C.; Carretero-Gonzalez, J.; Raji, A.-R. O.; Trease, N. M.; Grey, C. P. Direct Observation of Ion Dynamics in Supercapacitor Electrodes Using in situ Diffusion NMR Spectroscopy. *Nat. Energy* **2017**, *2*, 16216.

(5) Rodriguez, J.; Elola, M. D.; Laria, D. Polar Mixtures Under Nanoconfinement. *J. Phys. Chem. B* **2009**, *113*, 12744–12749.

(6) Kondrat, S.; Wu, P.; Qiao, R.; Kornyshev, A. A. Accelerating Charging Dynamics in Subnanometre Pores. *Nat. Mater.* **2014**, *13*, 387.

(7) Chmiola, J.; Yushin, G.; Gogotsi, Y.; Portet, C.; Simon, P.; Taberna, P.-L. Anomalous Increase in Carbon Capacitance at Pore Sizes Less Than 1 Nanometer. *Science* **2006**, *313*, 1760–1763.

(8) Jackel, N.; Simon, P.; Gogotsi, Y.; Presser, V. Increase in Capacitance by Subnanometer Pores in Carbon. *ACS Energy Letters* **2016**, *1*, 1262–1265.

(9) Merlet, C.; Péan, C.; Rotenberg, B.; Madden, P. A.; Daffos, B.; Taberna, P.-L.; Simon, P.; Salanne, M. Highly Confined Ions Store Charge More Efficiently in Supercapacitors. *Nat. Commun.* **2013**, *4*, 2701.

(10) Jiang, D.-e.; Jin, Z.; Henderson, D.; Wu, J. Solvent Effect on the Pore-Size Dependence of an Organic Electrolyte Supercapacitor. *J. Phys. Chem. Lett.* **2012**, *3*, 1727–1731.

(11) Feng, G.; Qiao, R.; Huang, J.; Sumpter, B. G.; Meunier, V. Ion Distribution in Electrified Micropores and Its Role in the Anomalous Enhancement of Capacitance. *ACS Nano* **2010**, *4*, 2382–2390.

(12) Somers, S. A.; McCormick, A. V.; Davis, H. T. Superselectivity and Solvation Forces of a Two Component Fluid Adsorbed in Slit Micropores. *J. Chem. Phys.* **1993**, *99*, 9890–9898.

(13) Keffer, D.; Davis, H. T.; McCormick, A. V. Effect of Loading and Nanopore Shape on Binary Adsorption Selectivity. *J. Phys. Chem.* **1996**, *100*, 638–645.

(14) Mohanty, S.; McCormick, A. Prospects for Principles of Size and Shape Selective Separations Using Zeolites. *Chem. Eng. J.* **1999**, *74*, 1–14.

(15) Vanderlick, T.; Scriven, L.; Davis, H. Forces Between Solid Surfaces in Binary Solutions. *Colloids and Surfaces* **1991**, *52*, 9–34.

(16) Stukowski, A. Visualization and Analysis of Atomistic Simulation Data with OVITO–the Open Visualization Tool. *Modell. Simul. Mater. Sci. Eng.* **2009**, *18*, 015012.

(17) Fang, A.; Smolyanitsky, A. Simulation Study of the Capacitance and Charging Mechanisms of Ionic Liquid Mixtures near Carbon Electrodes. *J. Phys. Chem. C* **2019**, *123*, 1610–1618.

(18) Frenkel, D.; Smit, B. *Understanding Molecular Simulation: From Algorithms to Applications*, 2nd ed.; Elsevier, 2002.

(19) Neal, J. N.; Van Aken, K.; Gogotsi, Y.; Wesolowski, D. J.; Wu, J. Self-Amplified Surface Charging and Partitioning of Ionic Liquids in Nanopores. *Phys. Rev. Appl.* **2017**, *8*, 034018.

(20) Bazant, M. Z.; Kilic, M. S.; Storey, B. D.; Ajdari, A. Towards an Understanding of Induced-Charge Electrokinetics at Large Applied Voltages in Concentrated Solutions. *Adv. Colloid Interface Sci.* **2009**, *152*, 48–88.

(21) Flory, P. J. Thermodynamics of High Polymer Solutions. *J. Chem. Phys.* **1942**, *10*, 51–61.

(22) Tresset, G. Generalized Poisson-Fermi Formalism for Investigating Size Correlation Effects with Multiple Ions. *Phys. Rev. E* **2008**, *78*, 061506.

(23) Fredrickson, G. H.; Liu, A. J.; Bates, F. S. Entropic Corrections to the Flory-Huggins Theory of Polymer Blends: Architectural and Conformational Effects. *Macromolecules* **1994**, *27*, 2503–2511.

(24) Lian, C.; Liu, K.; Van Aken, K. L.; Gogotsi, Y.; Wesolowski, D. J.; Liu, H.; Jiang, D.; Wu, J. Enhancing the Capacitive Performance of Electric Double-Layer Capacitors with Ionic Liquid Mixtures. *ACS Energy Letters* **2016**, *1*, 21–26.

(25) Forse, A. C.; Griffin, J. M.; Merlet, C.; Bayley, P. M.; Wang, H.; Simon, P.; Grey, C. P. NMR Study of Ion Dynamics and Charge Storage in Ionic Liquid Supercapacitors. *J. Am. Chem. Soc.* **2015**, *137*, 7231–7242.

(26) Smith, A. M.; Lee, A. A.; Perkin, S. Switching the Structural Force in Ionic Liquid-Solvent Mixtures by Varying Composition. *Phys. Rev. Lett.* **2017**, *118*, 096002.

(27) Coles, S. W.; Smith, A. M.; Fedorov, M. V.; Hausen, F.; Perkin, S. Interfacial Structure and Structural Forces in Mixtures of Ionic Liquid with a Polar Solvent. *Faraday Discuss.* **2017**, *206*, 427–442.

(28) Fukano, M.; Fujimori, T.; Segalini, J.; Iwama, E.; Taberna, P.-L.; Iiyama, T.; Ohba, T.; Kanoh, H.; Gogotsi, Y.; Simon, P.; Kaneko, K. Vertically Oriented Propylene Carbonate Molecules and Tetraethyl Ammonium Ions in Carbon Slit Pores. *J. Phys. Chem. C* **2013**, *117*, 5752–5757.

(29) Wang, Z.; Yang, Y.; Olmsted, D. L.; Asta, M.; Laird, B. B. Evaluation of the Constant Potential Method in Simulating Electric Double-Layer Capacitors. *J. Chem. Phys.* **2014**, *141*, 184102.

(30) Merlet, C.; Péan, C.; Rotenberg, B.; Madden, P. A.; Simon, P.; Salanne, M. Simulating Supercapacitors: Can We Model Electrodes as Constant Charge Surfaces? *J. Phys. Chem. Lett.* **2012**, *4*, 264–268.

(31) Yang, J.; Bo, Z.; Yang, H.; Qi, H.; Kong, J.; Yan, J.; Cen, K. Reliability of Constant Charge Method for Molecular Dynamics Simulations on EDLCs in Nanometer and Sub-Nanometer Spaces. *ChemElectroChem* **2017**, *4*, 2486–2493.

(32) Plimpton, S. Fast Parallel Algorithms for Short-Range Molecular Dynamics. *J. Comput. Phys.* **1995**, *117*, 1–19.

(33) Brown, W. M.; Wang, P.; Plimpton, S. J.; Tharrington, A. N. Implementing Molecular Dynamics on Hybrid High Performance Computers – Short Range Forces. *Comput. Phys. Commun.* **2011**, *182*, 898–911.

(34) Brown, W. M.; Kohlmeyer, A.; Plimpton, S. J.; Tharrington, A. N. Implementing Molecular Dynamics on Hybrid High Performance Computers – Particle-Particle Particle-Mesh. *Comput. Phys. Commun.* **2012**, *183*, 449–459.

(35) Martínez, L.; Andrade, R.; Birgin, E. G.; Martínez, J. M. PACKMOL: A Package for Building Initial Configurations for Molecular Dynamics Simulations. *J. Comput. Chem.* **2009**, *30*, 2157–2164.

(36) Doherty, B.; Zhong, X.; Gathiaka, S.; Li, B.; Acevedo, O. Revisiting OPLS Force Field Parameters for Ionic Liquid Simulations. *J. Chem. Theory Comput.* **2017**, *13*, 6131–6145.

(37) Nikitin, A. M.; Lyubartsev, A. P. New Six-Site Acetonitrile Model for Simulations of Liquid Acetonitrile and Its Aqueous Mixtures. *J. Comput. Chem.* **2007**, *28*, 2020–2026.

(38) Jorgensen, W. L.; Maxwell, D. S.; Tirado-Rives, J. Development and Testing of the OPLS All-Atom Force Field on Conformational Energetics and Properties of Organic Liquids. *J. Am. Chem. Soc.* **1996**, *118*, 11225–11236.

Graphical TOC Entry
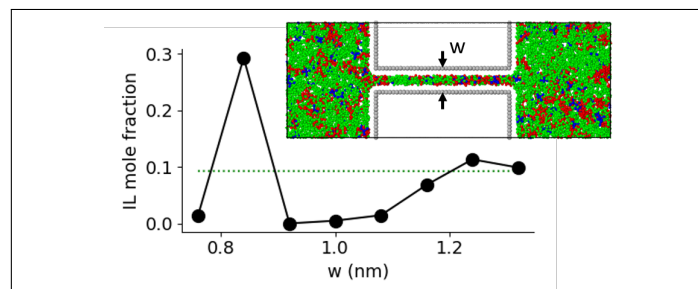
Supporting Information

Alta Fang[*] and Alex Smolyanitsky[*]

Applied Chemicals and Materials Division, National Institute of Standards and Technology, Boulder, CO 80305 USA

E-mail: alta.fang@nist.gov; alex.smolyanitsky@nist.gov

S1 Effects of varying in-pore region definition
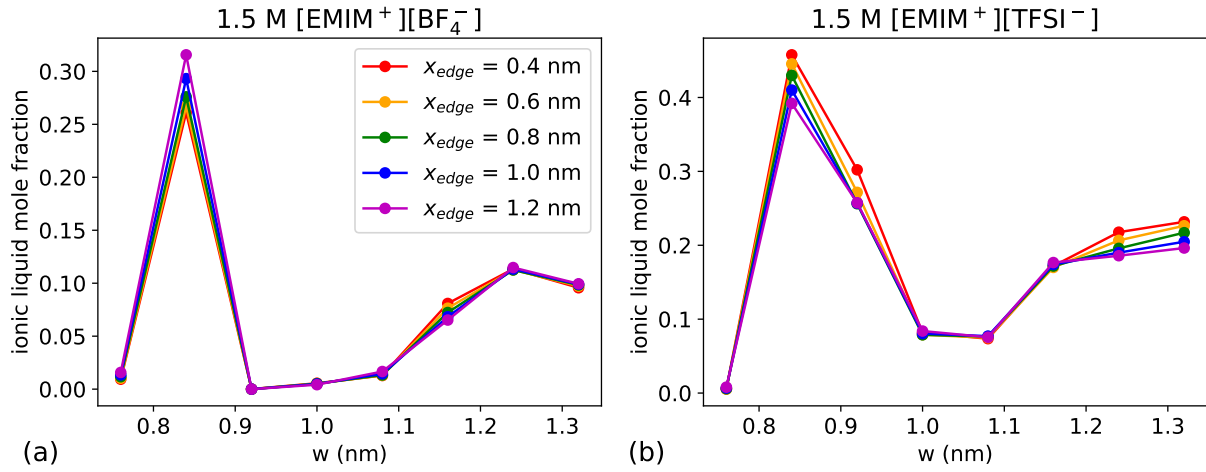
Figure S1: Simulated in-pore ionic liquid mole fractions calculated using different discarded lengths x_{edge} from the pore mouth on each side, for (a) 1.5 M [EMIM$^+$][BF$_4^-$] and (b) 1.5 M [EMIM$^+$][TFSI$^-$] in acetonitrile. The same legend applies to both subplots. The value of x_{edge} does not have a significant effect on the calculated in-pore ionic liquid mole fractions.

S2 Top-down views of mixtures inside the slit pores
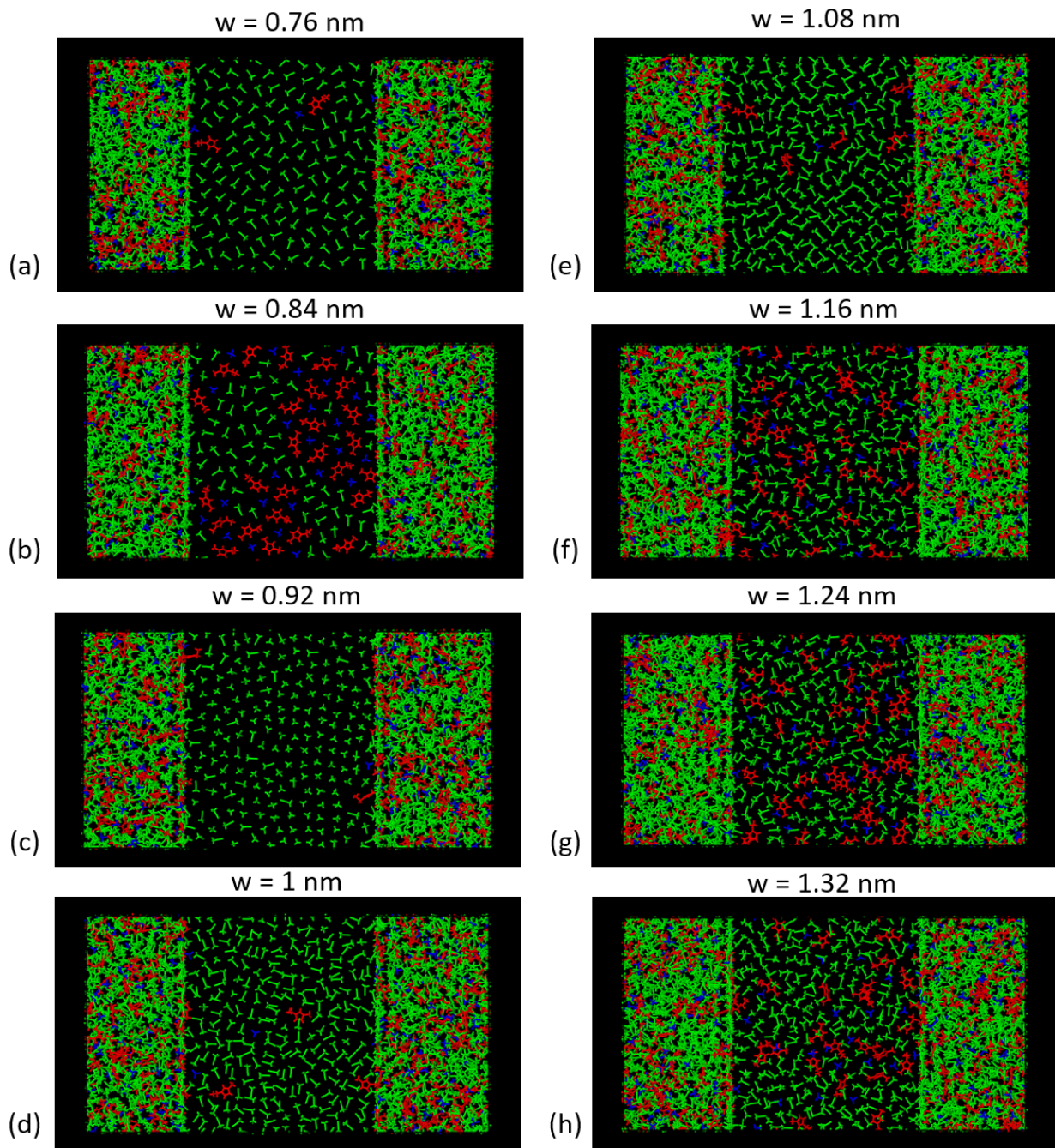
Figure S2: Top-down view of acetonitrile (green), EMIM$^+$ (red), and BF$_4^-$ (blue) in final simulation configurations for 1.5 M [EMIM$^+$][BF$_4^-$] in acetonitrile. The slit pore confinement region is in the center, and pore widths are (a) 0.76 nm, (b) 0.84 nm, (c) 0.92 nm, (d) 1 nm, (e) 1.08 nm, (f) 1.16 nm, (g) 1.24 nm, and (h) 1.32 nm.
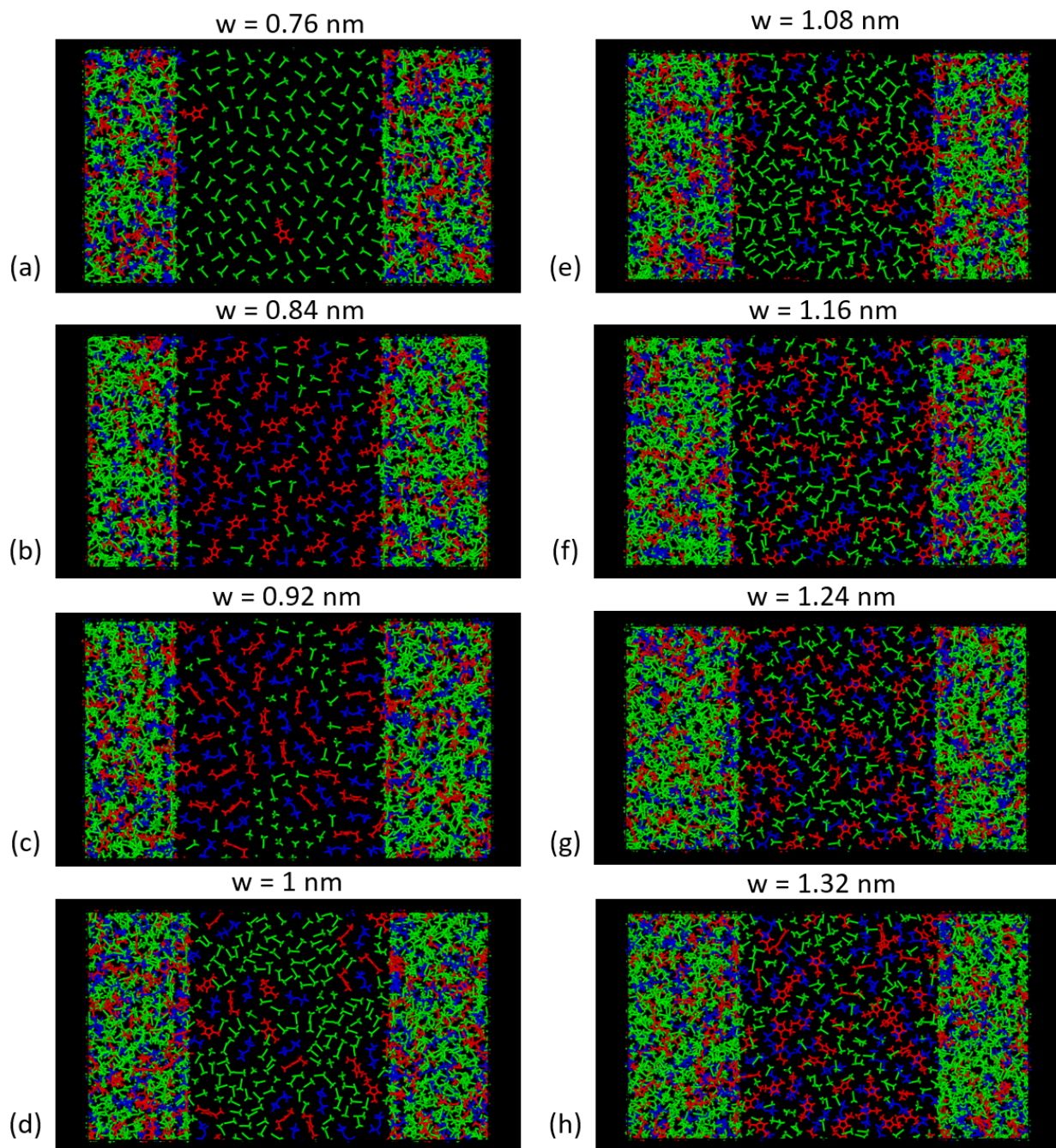
Figure S3: Top-down view of acetonitrile (green), EMIM$^+$ (red), and TFSI$^-$ (blue) in final simulation configurations for 1.5 M [EMIM$^+$][TFSI$^-$] in acetonitrile. The slit pore confinement region is in the center, and pore widths are (a) 0.76 nm, (b) 0.84 nm, (c) 0.92 nm, (d) 1 nm, (e) 1.08 nm, (f) 1.16 nm, (g) 1.24 nm, and (h) 1.32 nm.

S3   Effects on predicted $X_{\text{IL}}(w)$ of varying $\Delta\mu^\infty$, varying α, using bulk molar volumes
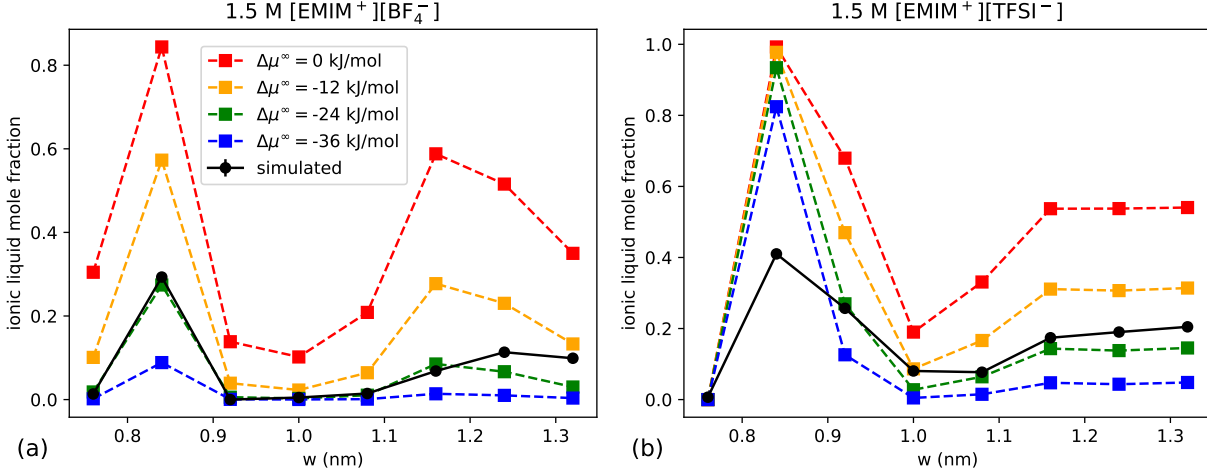

Figure S4:   Theoretically predicted in-pore ionic liquid mole fraction for various values of $\Delta\mu^\infty$ as a function of pore width (squares), along with data from MD simulations (black circles), for (a) 1.5 M [EMIM$^+$][BF$_4^-$] and (b) 1.5 M [EMIM$^+$][TFSI$^-$] in acetonitrile. The same legend applies to both subplots. The predicted trend remains qualitatively the same as $\Delta\mu^\infty$ varies. Values used for $\Delta\mu^\infty$ in the main text, which were estimated from the bulk limit, were -15.1 kJ/mol for 1.5 M [EMIM$^+$][BF$_4^-$] and -11.4 kJ/mol for 1.5 M [EMIM$^+$][TFSI$^-$].
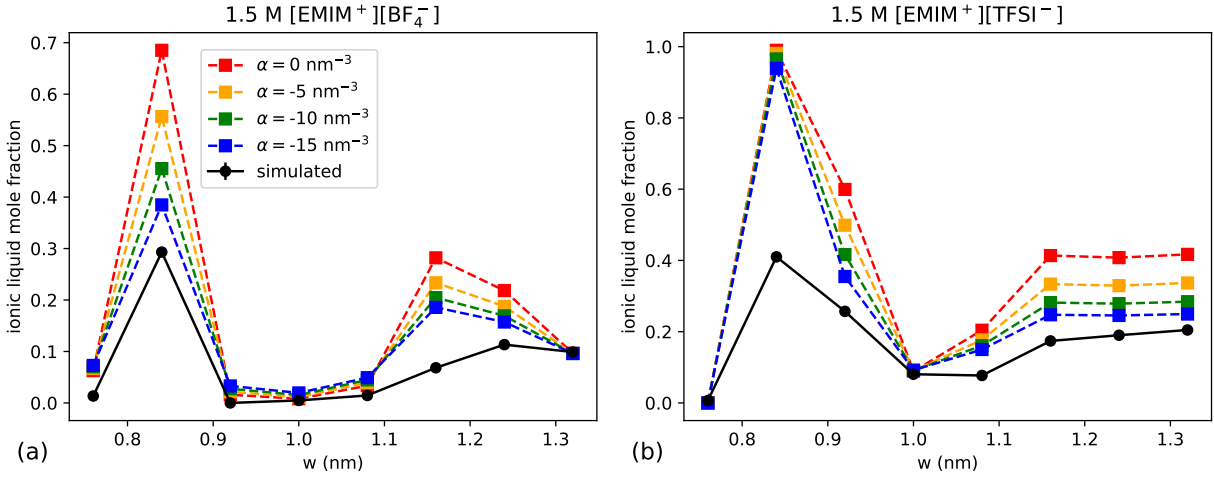
Figure S5: Theoretically predicted in-pore ionic liquid mole fraction for various values of α as a function of pore width (squares), along with data from MD simulations (black circles), for (a) 1.5 M [EMIM$^+$][BF$_4^-$] and (b) 1.5 M [EMIM$^+$][TFSI$^-$] in acetonitrile. The same legend applies to both subplots. The predicted trend remains qualitatively the same as α varies. Values used for α in the main text were -8 nm^{-3} for 1.5 M [EMIM$^+$][BF$_4^-$] and -6 nm^{-3} for 1.5 M [EMIM$^+$][TFSI$^-$].
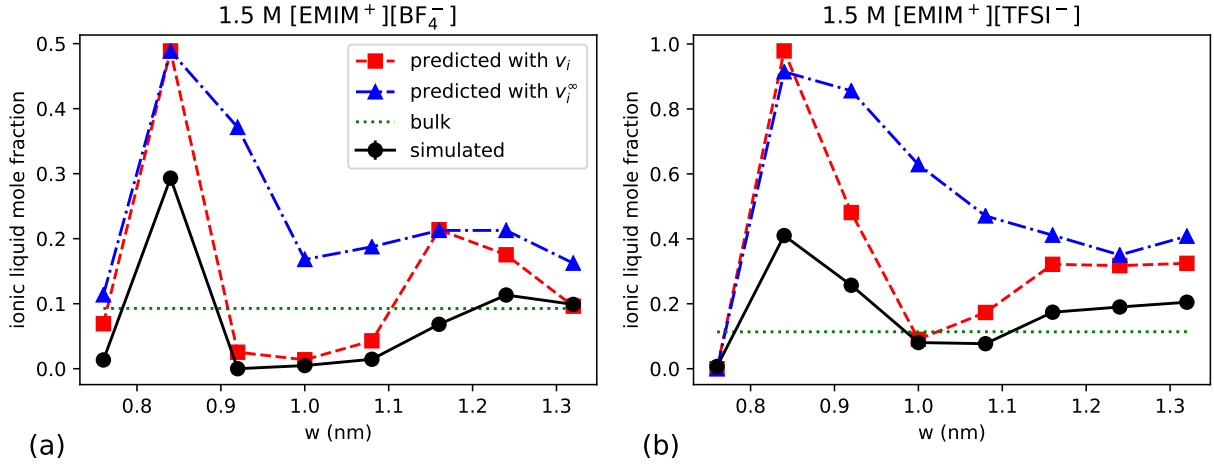

Figure S6: Theoretically predicted in-pore ionic liquid mole fraction as a function of pore width using v_i from MD simulations of liquids in confinement (red squares) or using constant bulk molar volumes for v_i (blue triangles), along with data from MD simulations (black circles), for (a) 1.5 M [EMIM$^+$][BF$_4^-$] and (b) 1.5 M [EMIM$^+$][TFSI$^-$] in acetonitrile. The same legend applies to both subplots. The bulk ionic liquid mole fractions are shown as green dotted lines for comparison.

S4 Model for $U_i(w)$ for pores containing up to two liquid layers

We develop an expression for the average per-molecule pore wall interaction energy $U_i(w)$ for each species i in the regime of pore width w where pores can accommodate up to two layers of liquid molecules. The interaction energy between a molecule and a single flat wall can be modeled by integrating the Lennard-Jones potential over half-space[1] to yield

$$U(z) = 2\pi\varepsilon \left[\frac{2}{45} \left(\frac{\sigma}{z}\right)^9 - \frac{1}{3} \left(\frac{\sigma}{z}\right)^3 \right], \tag{S1}$$

where z is the distance of a molecule from the wall, ε determines the strength of the interaction energy, and $\sigma = \left(\frac{5}{2}\right)^{1/6} z_{min}$, where z_{min} is the value of z at which $U(z)$ achieves its minimum value.

To model the total average per-molecule interaction energy with both pore walls, we assume that for a pore sufficiently narrow to contain only one layer of liquid (that is, $w < 2\sigma$), molecules reside at the center of the pore, while for $2\sigma \leq w < 2\sigma + 2d$, where d is the diameter of the molecule, each molecule resides at a distance σ from one of the pore walls. Thus, the total average per-molecule interaction energy with the pore can be modeled by

$$U_i(w) = \begin{cases} 4\pi\varepsilon_i \left[\dfrac{2}{45} \left(\dfrac{\sigma_i}{w/2}\right)^9 - \dfrac{1}{3} \left(\dfrac{\sigma_i}{w/2}\right)^3 \right] & \text{for } w < 2\sigma_i \\[2ex] 2\pi\varepsilon_i \left[\dfrac{2}{45} - \dfrac{1}{3} + \dfrac{2}{45} \left(\dfrac{\sigma_i}{w - \sigma_i}\right)^9 - \dfrac{1}{3} \left(\dfrac{\sigma_i}{w - \sigma_i}\right)^3 \right] & \text{for } 2\sigma_i \leq w < 2\sigma_i + 2d_i. \end{cases} \tag{S2}$$

Using σ_i and ε_i as fitting parameters, we use nonlinear least squares regression to fit Eq. S2 to the values of $U_i(w)$ obtained from MD simulations, yielding the values in Table S1. We have assumed that all of our simulations lie within the domain of applicability of Eq. S2.

Table S1: Values of σ_i and ε_i obtained by fitting Eq. S2 to simulated $U_i(w)$ for 1.5 M [EMIM$^+$][BF$_4^-$] or 1.5 M [EMIM$^+$][TFSI$^-$] in acetonitrile. Fitting is done using nonlinear least squares regression.

1.5 M [EMIM$^+$][BF$_4^-$]			1.5 M [EMIM$^+$][TFSI$^-$]		
	σ_i (nm)	ε_i (kJ/mol)		σ_i (nm)	ε_i (kJ/mol)
ACN	0.42	9.0	ACN	0.41	9.3
EMIM$^+$	0.43	22.7	EMIM$^+$	0.42	23.7
BF$_4^-$	0.47	6.3	TFSI$^-$	0.47	24.8

S5 Discussion of using total energy and per-area wall interaction energy in the analytical theory

The total excess Gibbs energy of a liquid inside a pore relative to the bulk may be written by summing the liquid-wall interaction energies and the Gibbs energy associated with the liquid:

$$G_{tot} = A \sum_{i \in \{0,+,-\}} \tilde{U}_i c_i v_i \tag{S3}$$

$$+ Aw \left(k_B T \left[\sum_{i \in \{0,+,-\}} c_i \ln(c_i v_i) + \alpha c_0 v_0 c_{\mathrm{IL}} v_{\mathrm{IL}} \right] - \sum_{i \in \{0,+,-\}} \mu_i^{\infty} c_i \right).$$

Here, A is the area of the slit pore, $\tilde{U}_i$ is the per-area pore wall interaction energy of species i, and the other variables are as defined in the main text. Minimizing G_{tot} with respect to the in-pore concentration of ionic liquid yields

$$
\begin{aligned}
0 &= \frac{dG_{tot}}{dc_{\mathrm{IL}}} \tag{S4} \\
&= \frac{v_{\mathrm{IL}}}{w}(-\tilde{U}_0 + \tilde{U}_{\mathrm{IL}}) \\
&\quad + k_B T \left[2 + \ln(c_{\mathrm{IL}} v_+) + \ln(c_{\mathrm{IL}} v_-) - \frac{v_{\mathrm{IL}}}{v_0} \ln(1 - c_{\mathrm{IL}} v_{\mathrm{IL}}) - \frac{v_{\mathrm{IL}}}{v_0} + \alpha v_{\mathrm{IL}}(1 - 2c_{\mathrm{IL}} v_{\mathrm{IL}}) \right] \\
&\quad - \Delta\mu^{\infty},
\end{aligned}
$$

which can then be used to obtain X_{IL} as described in the main text. Figure S7 shows $\tilde{U}_i(w)$ for each liquid extracted from separate MD simulations of pure solvent or pure ionic liquid in confinement. Figure S8 shows that Eq. S4 reproduces the qualitative behavior of the simulations well when the actual values of $\tilde{U}_i$ at each pore width are used, but using a single average value for $\tilde{U}_i$ for each liquid leads to poor predictions. The variations in $\tilde{U}_i$ with w are due to the particular packing behavior of the in-pore molecules (reflecting the variations of the effective molar volume v_i), suggesting these effects play an important role in determining the in-pore mixture composition.
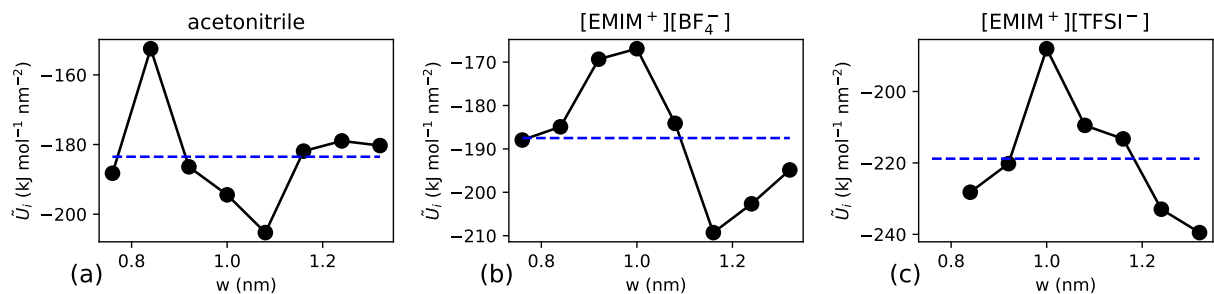
Figure S7: Per-area pore wall interaction energies of (a) acetonitrile, (b) $[\text{EMIM}^+][\text{BF}_4^-]$, and (c) $[\text{EMIM}^+][\text{TFSI}^-]$. The average values are shown as blue dashed lines.
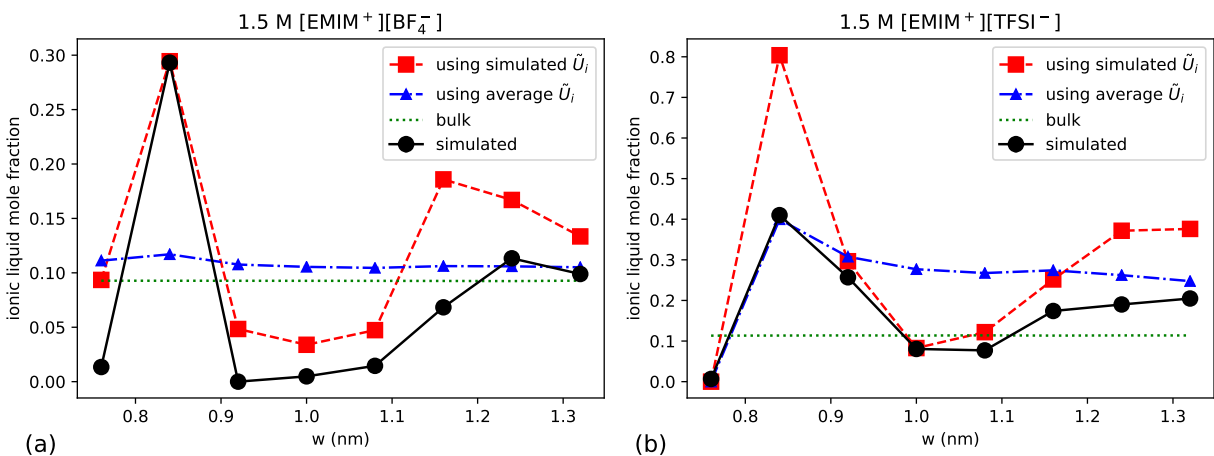

Figure S8: Theoretically predicted in-pore ionic liquid mole fraction as a function of pore width using $\tilde{U}_i$ from MD simulations of each liquid in confinement (red squares) or using a constant average value for $\tilde{U}_i$ (blue triangles), along with data from MD simulations (black circles), for (a) 1.5 M $[\text{EMIM}^+][\text{BF}_4^-]$ and (b) 1.5 M $[\text{EMIM}^+][\text{TFSI}^-]$ in acetonitrile. The same legend applies to both subplots. The bulk ionic liquid mole fractions are shown as green dotted lines for comparison.
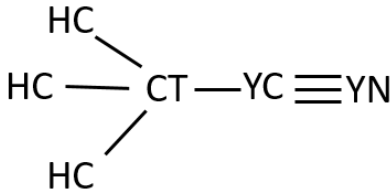
S6 Force field parameters for acetonitrile

Figure S9: Atom types for acetonitrile force field.

To model acetonitrile, we used the force field parameters in Tables S2 and S3, where atom types are defined as shown in Fig. S9.

Table S2: Force field parameters for atoms in acetonitrile.

atom	mass (g/mol)	charge (e)	σ (nm)	ε (kJ/mol)
YN	14.007	-0.5126	0.301124	0.5569
YC	12.011	0.4917	0.354578	0.56107
CT	12.011	-0.5503	0.34	0.45773
HC	1.008	0.1904	0.26495	0.06569

Table S3: Force field parameters for bonds and angles in acetonitrile, where the bond energy is $E = K_r(r - r_0)^2$ and the angle energy is $E = K_\theta(\theta - \theta_0)^2$.

bond	r_0 (nm)	K_r (kJ mol^{-1} nm^{-2})
YN-YC	0.1157	251040
YC-CT	0.1458	167360
CT-HC	0.109	142256
angle	θ_0 (degrees)	K_θ (kJ mol^{-1} rad^{-2})
CT-YC-YN	180	334.75
HC-CT-YC	110	146.44
HC-CT-HC	109.5	146.44

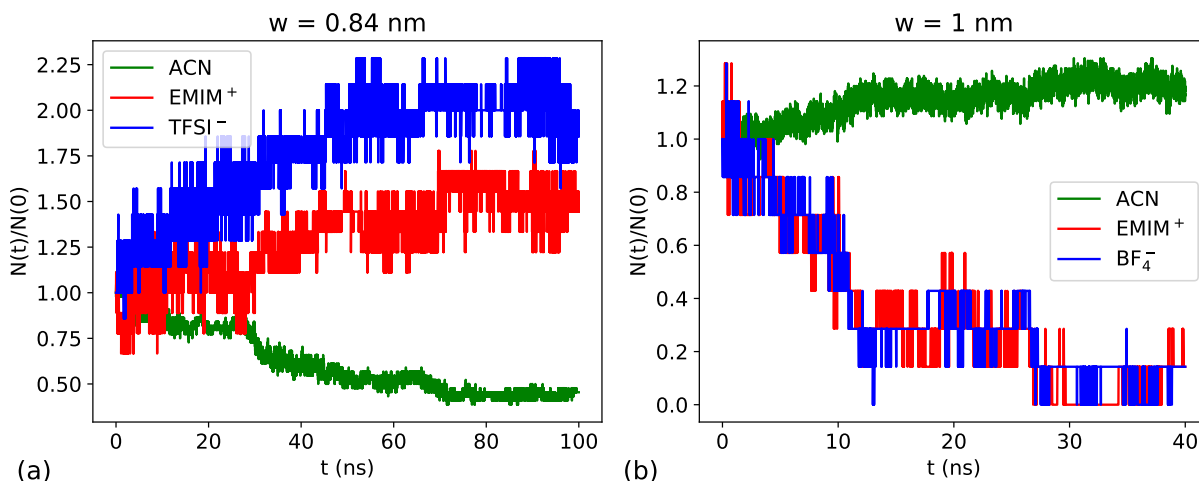# S7   Examples of time evolution of in-pore species counts

Figure S10:   In-pore count of each species as a function of simulated time, normalized by each count at $t = 0$. Here, $t = 0$ is the time at which the NVT simulations begin, after 2 ns of simulation in the NPT ensemble. (a) 1.5 M [EMIM$^+$][TFSI$^-$] in acetonitrile confined in a pore of $w = 0.84$ nm requires 100 ns of simulation time to appear to reach steady state. (b) 1.5 M [EMIM$^+$][BF$_4^-$] in acetonitrile confined in a pore of $w = 1$ nm appears to exhibit a plateau in in-pore populations within 40 ns.

References

(1) Forsman, J.; Woodward, C. E.; Trulsson, M. A Classical Density Functional Theory of Ionic Liquids. *J. Phys. Chem. B* **2011**, *115*, 4606–4612.